Applied Surface Science 688 (2025) 162309

Contents lists available at ScienceDirect

Applied Surface Science

journal homepage: www.elsevier.com/locate/apsusc

Full Length Article

Selective trace bromide ion removal from chloride ion-dominated solutions using defective Zr-based metal–organic frameworks☆

WooYeon Moon [a], Dong Gyu Park [b], Younghu Son [c], Minyoung Yoon [c,**], Kyung Min Choi [a,b,*]

[a] Department of Chemical and Biological Engineering, Sookmyung Women's University, 100 Cheongpa-ro 47 gil, Yongsan-gu, Seoul, 04310, Republic of Korea
[b] Institute of Advanced Materials and Systems, Sookmyung Women's University, Seoul 04310, Republic of Korea
[c] KNU G-LAMP Research Center, KNU Institute of Basic Sciences and Department of Chemistry, Kyungpook National University, 80 Daehakro, Bukgu, Daegu, 41566, Republic of Korea

ARTICLE INFO

Keywords:
Bromide ion removal
Defect site
Metal–organic framework
Ion-exchange
Ion-adsorption
Chloride ion
Trace pollutant

ABSTRACT

The removal of bromide ions (Br^-) from water is critical, as these ions can generate bromate and brominated disinfection by-products that are toxic, carcinogenic, and corrosive. Previous research has not focused on the removal of Br^- from water with a heavy presence of chloride ions (Cl^-). To address this research gap, we proposed a defective Zr-based metal–organic framework (MOF) to selectively remove trace Br^- in environments with high concentrations of Cl^-. We demonstrated that the open acidic sites on the secondary building units in a defective Zr-based MOF-808 (MOF-808-Cl) selectively removed the trace Br^- in the presence of high concentration of Cl^- using varying degrees of electrostatic interactions induced by their own polarizability. The Br^- removal was performed with the mixed mechanism of ion-exchange and -adsorption, with contributions of approximately 70% and 30%, respectively. The Br^- was successfully removed when the concentration of Cl^- was 100 times higher than that of Br^-. Our findings demonstrate the potential of MOF-808-Cl for industrial applications requiring trace ion removal and can provide insights for future research on selective ion removal in a competitive environment.

1. Introduction

The removal of bromide ions (Br^-) from water is emerging as a critical concern due to its potential for generating bromate and brominated disinfection by-products, which are toxic, carcinogenic, and corrosive in nature [1–5]. Several processes such as membrane (reverse osmosis [6], electrodialysis [7]), electrochemical (electrolysis [8], capacitive deionization [9,10]), and adsorption methods (activated carbon [11,12], zeolite [13], ion exchange resin [14,15], and coagulation [16]) can be used to remove Br^- from water. Nevertheless, these methods encounter substantial challenges when deployed in chloride-dominated contexts, which are prevalent in industries requiring high-purity salts such as pharmaceuticals, dialysis solutions, water treatment, food processing, chemical manufacturing, and semiconductor fabrication [17–21]. Particularly in water chlorination, the electrolysis of saltwater can result in bromate formation even with trace Br^- ions, thus potentially resulting in serious public health risks in drinking water [22]. The primary challenge in the removal of Br^- from Cl^--dominated condition is that the chemical and physical properties of both ions become less distinct in high concentrations of these competing ions (Table 1) [23]. Therefore, it is imperative to devise effective methodologies for differentiating between similar ions, which ultimately facilitate the removal of Br^- from Cl^--rich salt solutions. In this study, we showed that a defective Zr-based metal–organic framework (MOF) can selectively remove trace Br^- in high concentrations of Cl^- using different degree of electrostatic interaction induced by their own

Abbreviations: MOFs, metal–organic frameworks; DMF, *N,N*-dimethylformamide; PVB, polyvinyl butyral; SCXRD, Single-Crystal X-ray diffraction; PXRD, Powder X-ray diffraction; IC, Ion chromatography; BET, Brunauer–Emmett–Teller; ICP-OES, Inductively coupled plasma optical emission spectrometer.

☆ This article is part of a special issue entitled: 'MCARE 2024_APSUSC' published in Applied Surface Science.

* Corresponding author at: Department of Chemical and Biological Engineering, Sookmyung Women's University, 100 Cheongpa-ro 47 gil, Yongsan-gu, Seoul, 04310, Republic of Korea.
** Corresponding author.
E-mail addresses: myyoon@knu.ac.kr (M. Yoon), kmchoi@sookmyung.ac.kr (K.M. Choi).

https://doi.org/10.1016/j.apsusc.2025.162309
Received 29 October 2024; Received in revised form 24 December 2024; Accepted 3 January 2025
Available online 4 January 2025

Table 1
Comparison of Cl and Br.

	Cl^-	Br^-
Hydrated radius [10^{-10} m]	0.332	0.330
Ionic radius [10^{-10} m]	0.181	0.198
Polarizability [10^{-30} m^3]	3.42	4.85

polarizability [24–33]. Specifically, the defective MOF-808-Cl (Zr_6(trimesate)$_2$(formate)$_6$(OH)$_4$(μ^3-O)$_2$$Cl_2$) was chosen for the trace Br^- removal, as it has both Lewis and Brønsted acidic sites on its uncoordinated sites of secondary building units and Cl^- counter-ions on its defective sites (Fig. 1) [34–36]. Its structure and counter-ion position were characterized using single crystal X-ray diffraction and a compositional analysis. The efficacy of MOF-808-Cl in removing Br^- was evaluated using ion chromatography (IC). The powder and pelletized MOF samples were tested for Br^- removal efficiency in both immersion and penetration systems. We founded that MOF-808-Cl effectively removed the Br^- in both immersion and penetration conditions, regardless of it forms. The Br^- removal was performed via the mixed mechanism of ion-exchange and -adsorption, whose contributions were calculated to be approximately 70 % and 30 %, respectively. Then, it was proven that the Br^- was removed in the presence of Cl^--dominated solutions using both powder and pelletized form in conditions of immersion and penetration. The Br^- was successfully removed even when the concentration of Cl^- was 100 times higher than that of Br^-.

Previous studies have shown that MOFs can remove Br^- in aqueous media [19,25]. However, these approaches have focused on structural and functional designs of MOFs for removing Br^- solely from Br^--only or -rich environments. To address this research gap, our study focused on using the defect sites of MOFs to selectively remove Br^- from Cl^--dominated environments using both vacant-site adsorption and substitutional methods. Moreover, we also sought to determine the removal mechanisms and kinetics along with a detailed structural analysis to distinguish our approach those of from previous reports.

2. Methods

2.1. Materials

Zirconium(IV) oxychloride octahydrate ($ZrOCl_2 \cdot 8H_2O$), trimesic acid (H_3BTC), acetic acid, formic acid, *N,N*-dimethylformamide (DMF), the bromide standard for IC, the chloride standard for IC, and Sigmacote® were purchased from Sigma-Aldrich (USA). Acetone, ethyl alcohol (EtOH), and water (HPLC grade) were purchased from Duksan (Republic of Korea). Poly(vinyl butyral) (PVB) was purchased from Aladdin (USA). All the reagents were used without further purification except for the materials used in the IC.

2.2. Material preparation

2.2.1. Synthesis of MOF-808-Cl

MOF-808-Cl was prepared using an aqueous reflux method. In a 250 mL round-bottom flask, zirconium(IV) oxychloride octahydrate (5.9 g, 3.4 mmol) and trimesic acid (1.1 g, 5.2 mmol) were dissolved in deionized water (14.02 mL). Acetic acid (2.95 mL) was added as a modulator. The mixture was heated to 97 °C and maintained under reflux with vigorous stirring for 12 h. Following the reaction, the resulting white suspension was separated and washed with deionized water. MOF-808-Cl powder was obtained by drying the product in a vacuum oven at 75 °C overnight.

2.2.2. Pelletization of MOF-808-Cl

The MOF powder was pelletized using PVB (M.W. 90,000–120,000) as the binder [37–39]. First, PVB (4.0 g) was dissolved in ethanol via sonication until a transparent solution was obtained. The MOF-808-Cl powder (40 g) was added to the PVB solution. The mixture was then thoroughly blended using a planetary mixer to obtain a homogeneous white slurry. To ensure an optimal viscosity for extrusion, the slurry was adjusted through drying in a 60 °C oven or adding more ethanol as needed. The prepared slurry was extruded into uniform strands and cut into the desired lengths. These extruded pellets were vacuum-dried at 75 °C overnight to remove any remaining solvent, resulting in well-formed MOF-808-Cl pellets.

2.2.3. Synthesis of MOF-808-Cl single crystal

To analyze the structure of the MOF-808-Cl using single crystal X-ray diffraction, it was synthesized as a single crystal. Before the synthesis, the inner surface of a 20 mL glass vial was treated with Sigmacote® siliconizing reagent, thoroughly washed with acetone, and dried in an oven at 100 °C for 1 h. This process was intended to minimize nucleation during crystal growth. In the prepared vial, zirconium oxychloride octahydrate (0.032 g, 0.10 mmol) and trimesic acid (0.022 g, 0.10 mmol) were dissolved in 2.0 mL of DMF and 4.0 mL of formic acid. The mixture was then heated at 100 °C oven for 7 d. After the reaction, the product was washed with DMF and acetone to yield visible individual crystals of MOF-808-Cl [40].

2.3. Characterization

The surface morphology and particle size of the MOF-808-Cl powder and pellets were examined using field-emission scanning electron

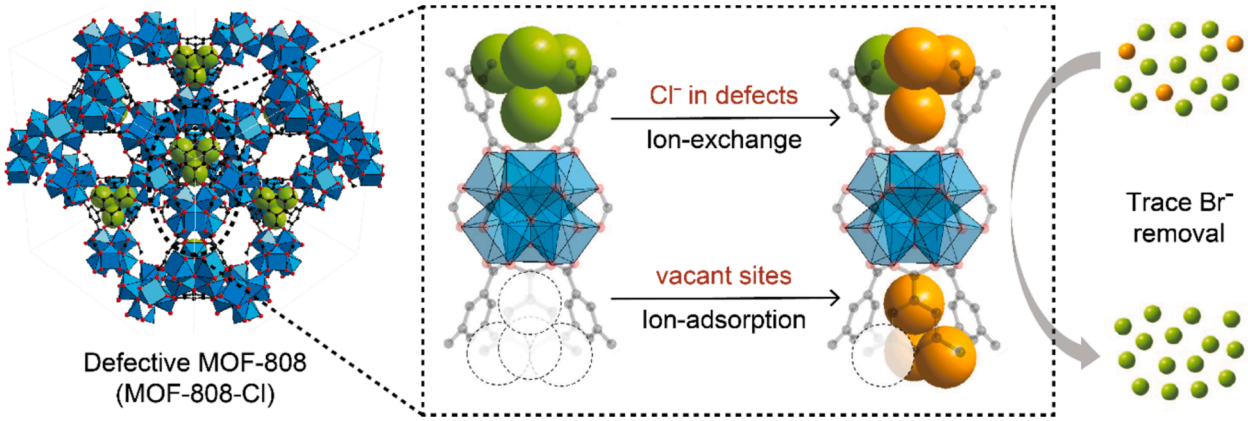

Fig. 1. Schematic illustration showing the trace Br^- removal mechanism *via* both ion-exchange and ion-adsorption within the defective MOF-808 (MOF-808-Cl) structure. Zr: blue, C: black, O: red, Cl: green, Br: orange. (For interpretation of the references to colour in this figure legend, the reader is referred to the web version of this article.)

microscopy (JEM-7600F, JEOL) at the Chronic and Metabolic Diseases Research Center of Sookmyung Women's University. Powder samples were dispersed in acetone and deposited onto a silicon wafer on the holder, whereas pelletized samples were mounted with copper tape to allow analyses of all sides and cross-sectional views. Scanning electron microscopy (SEM) imaging was performed in the GB_LOW mode with a scan voltage of 3.8 kV.

Powder X-ray diffraction (PXRD) patterns were obtained using a Bruker (Germany) D8 Advanced (TRIO/TWIN) instrument at 1.6 kW (40 kV and 40 mA) at the Chronic and Metabolic Diseases Research Center of Sookmyung Women's University. X-rays were scanned at 0.02°/min over a 2θ range from 3° to 40° using the silicon low background holders. The pelletized samples were ground into powder prior to measurement.

Nitrogen adsorption measurements were performed using a BELSORP-max gas adsorption analyzer (MicrotracBEL Corp.). Both powder and pellet samples were pretreated via evacuating at 75 °C for 24 h under a dynamic vacuum before analysis. Ultrahigh pure N_2 (99.999 %) was used for the N_2 gas sorption analysis.

An ion chromatography (IC) analysis was performed using a Dionex ICS-5000 system (Thermo Fisher Scientific, Waltham, MA, USA) equipped with a conductivity cell detector. Separation was performed using an analytical AS19 column (4 × 250 mm) at a flow rate of 1.0 mL/min. The mobile phase was generated using an Eluent Generator Cartridge (KOH), and the injection volume of samples was set at 25 μL.

Single-crystal diffraction data were obtained using the 2D SMC beamline at the Pohang Accelerator Laboratory, South Korea. The diffraction data were collected using a synchrotron radiation source (2D SMC with a silicon (111) double-crystal monochromator, λ = 0.80000 Å) on a Rayonix (USA) MX225HS CCD at low temperatures (100(2) K). The PAL BL2D SMDC program [41] was used for data collection (detector distance: 66 mm, omega scan; Δω = 1°, exposure time: 1 s per frame), and the HKL3000sm (ver. 703r) [42] software was used for cell refinement, reduction, and absorption correction. The crystal structure was predicted using direct methods and refined via full-matrix least-squares refinement using the SHELXL-2019 computer program [43]. The positions of all non-hydrogen atoms were refined using anisotropic displacement factors. All hydrogen atoms were placed using a riding model, and their positions were constrained relative to their parent atoms using the appropriate HFIX command. The crystallographic data and refinement results are summarized in Table S1. The supplementary crystallographic data for this study can be found in CCDC-2382956. The data can be obtained free of charge from https://www.ccdc.cam.ac.uk/conts/retrieving.html (or from the CCDC, 12 Union Road, Cambridge CB2 1EZ, UK; fax: +44 1223 336033; deposit@ccdc.cam.ac.uk).

2.4. Ion removal experiments

To test the Cl^- and Br^- ion removal performance of MOF-808-Cl, MOF samples were pre-treated in a vacuum oven at 75 °C overnight to remove any residual moisture and stabilize the samples. Depending on the experimental conditions, MOF powder or pellet samples were used. The solvent containing the ions was prepared by diluting 1,000 ppm Cl^- or Br^- standard solutions for IC. Furthermore, 10 mL of solvent was used in this study and contained either Br^- or Cl^- ions, or a mixture of both ions.

For the immersion tests, the MOF samples were soaked in each solvent in cylindrical tubes for 2 h or as specified. After the immersion, the supernatant was centrifuged to separate the MOF. For the penetration test, the MOF samples were packed into a 12 mL syringe fitted with a 0.22 μm PTFE filter, and the solvent was passed through and collected. After both processes, the remaining solution was filtered through a 0.22 μm PTFE filter before and after the final ion concentration analysis. The ion removal efficiency of MOF-808-Cl was calculated by comparing the remaining ion concentration with the initial concentration using ion chromatography. This value was calculated using the following equation:

$$Removal\ Efficiency(\%) = \frac{C_i - C_f}{C_i} \times 100 \quad (1)$$

where C_i is the initial ion concentration (ppm) and C_f is the residual ion concentration for each run. For Cl^-, C_f was determined by subtracting the baseline concentration C_b (the concentration of counter ion leached into water) from the concentration measured after the experiment.

Furthermore, for the sequential immersion test, the MOF was immersed in the solvent and centrifuged, and the supernatant was collected after each sequence, with the unexposed MOF added for subsequent sequences. For the sequential test of penetration, a syringe with a 0.22 μm PTFE filter containing MOF was used to inject the solvent, with the filtrate collected and an unexposed MOF filter assembly used for subsequent sequences. After each sequence, the remaining ion concentration was measured, and the ion removal efficiency of MOF-808-Cl was calculated through a comparison with the initial concentration.

3. Results and discussion

3.1. Characterization

MOF-808-Cl was synthesized using zirconium(IV) oxychloride octahydrate and trimesic acid in water under reflux. After washing with water and drying in the vacuum oven, the resulting MOF-808-Cl, obtained as a white powder, was shaped into pellets using PVB as a binder. PVB was dissolved in ethanol, and the MOF powder was added and mixed to form a white slurry. The slurry was then extruded into uniform strands and cut into pellets.

The morphology of the MOF-808-Cl powder and pellets were analyzed using SEM. As shown in the SEM images (Fig. 2a), the MOF-808-Cl particles were *ca.* 6.5 μm in diameter and octahedrally-shaped with eight facets. No side-products or organic residues were observed. After the extrusion process, the pellets were cylindrical with a diameter of approximately 2.5 mm and a height of approximately 2–3 mm (Fig. 2b and Fig. S1). The morphology of each MOF-808-Cl particle was maintained after pellet formation. Both the particles in the powder and pellet forms exhibited a similar size and morphology (Fig. S2).

The crystallinities of the MOF-808-Cl powder and pellets were evaluated using PXRD. The PXRD patterns of the MOF-808-Cl powder exhibited sharp, high-intensity peaks that aligned with the simulated pattern of MOF-808. The peaks at 4.35°, 8.33°, and 8.70° corresponded to the (111), (311), and (222) facets of the MOF-808 structure, respectively. These results confirmed the successful synthesis of MOF-808-Cl with high crystallinity and a structure consistent with MOF-808. The PXRD pattern of the resulting MOF-808-Cl pellets retained identical peak positions and intensities, indicating that the PVB binder used during pelletization did not affect the crystal structure of MOF-808-Cl (Fig. 2c). This observation confirmed that the extrusion process did not induce any loss of crystallinity. Additionally, the pellets exhibited stability in water without disassembling particles and losing crystallinity (Figs. S3 and S4). This dynamic occurred because both MOF-808-Cl and the PVB binder are not soluble in water and have a stable chemical structure. Therefore, MOF-808-Cl pellets can be used for robust functions in water.

The permanent porosity of the MOF-808-Cl was verified by measuring nitrogen gas sorption isotherms (Fig. 2d). The Brunauer–Emmett–Teller (BET) surface areas of MOF-808-Cl powder and pellets were 1464.3 and 1080.5 m^2/g, respectively. (Table S2). The amount of N_2 sorption and BET surface area of the pellet samples were lower than those of the powder samples. This difference occurred because the PVB binder attached to the surface of the crystals or occupied part of the pores in MOF-808-Cl. However, the average pore size of the pellets was similar to that of the powder, indicating that the function of the MOF-808-Cl micropores was expected to be similar in the pellets.

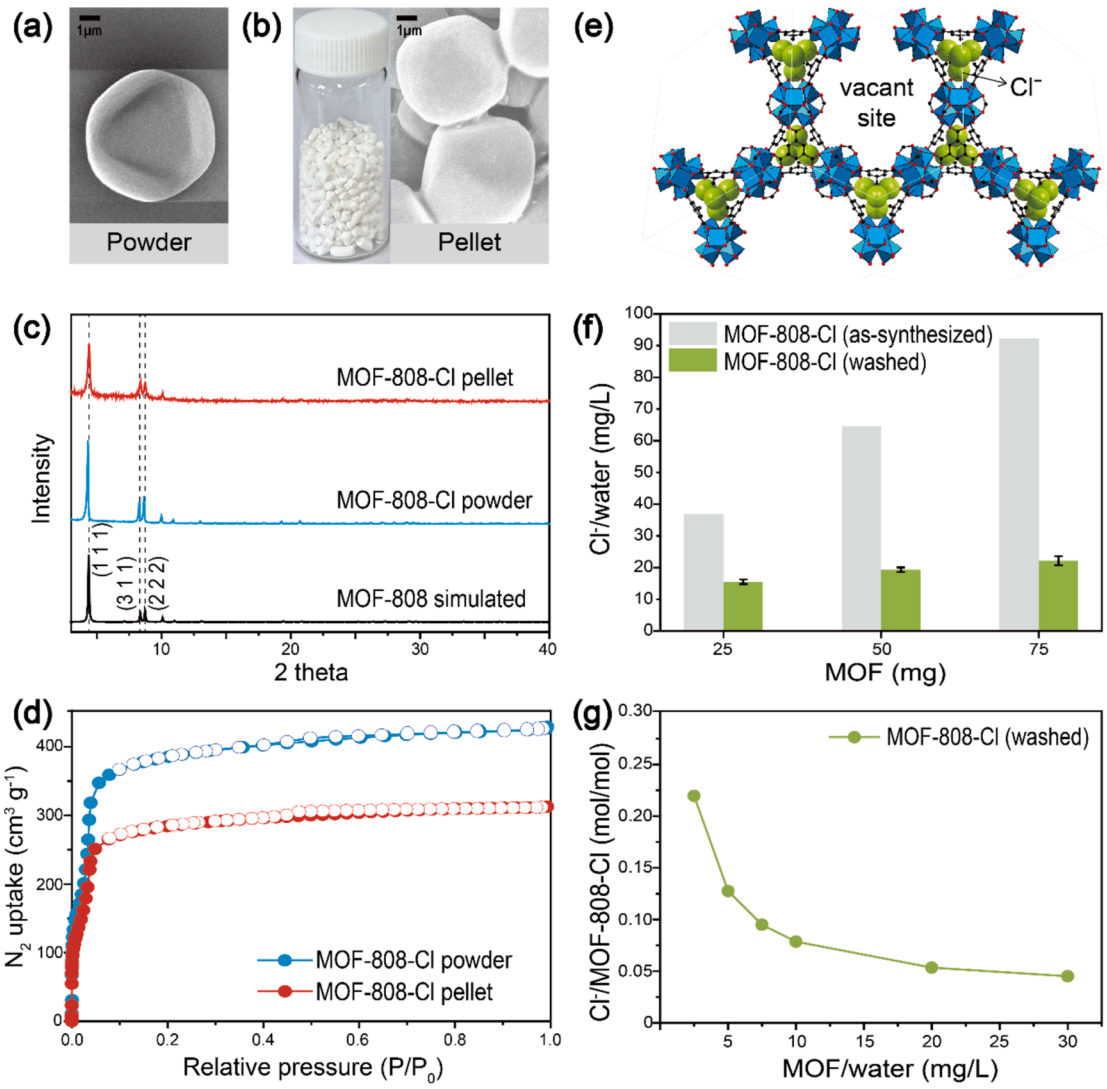

Fig. 2. Characterization of MOF-808-Cl. (a) SEM image of MOF-808-Cl powder. (b) Standard and SEM images of MOF-808-Cl pellet. (c) PXRD patterns of MOF-808-Cl powder and pellet. (d) N_2 adsorption isotherms at 77 K for MOF-808-Cl powder and pellet. (e) Crystal structure of MOF-808-Cl that resulted from its single crystal X-ray diffraction. Zr: blue, C: black, O: red, Cl: green, Br: orange. (f) Concentration of Cl^- within the MOF structure after washing MOF-808-Cl. (g) Amount of Cl^- released per mol of MOF-808-Cl with MOF concentration in water. (For interpretation of the references to colour in this figure legend, the reader is referred to the web version of this article.)

3.2. *Presence of Cl^- in MOF-808-Cl*

Counter-ions exist in the defective MOF-808 structure to balance the charge on the secondary building units [44–46]. A single crystal of MOF-808-Cl was prepared to be 40 μm in diameter and analyzed to determine its structure and compositions (Fig. S5). A single-crystal structure analysis suggested that vacant sites existed in the MOF due to occupancy refinement. Although most oxygen atoms had full occupancy, the μ^3-O atom had a smaller occupancy because of the defect sites in the MOF, resulting in the chemical formula $[Zr_2(trimesate)_{2/3}(formate)_2(OH)_2(\mu^3\text{-}O)_{2/3}]^{(2/3)+}$ (Table S1). Owing to the vacant sites (or defect sites) of the μ^3-O atom in the MOF, other counter-ions were expected to be present in the MOF to render the MOF charge-neutral. As $ZrOCl_2$ was used as a metal source of the MOF, the Cl^- present in the MOF was expected to be a counter-ion. The presence of Cl^- was confirmed by the IC experiment, and 2/3 of the Cl^- ion was added to the chemical formula to compensate for the charge balance of the framework. This addition resulted in the chemical formula of $[Zr_2(trimesate)_{2/3}(formate)_2(OH)_2(\mu^3\text{-}O)_{2/3}Cl_{2/3}]$, where the occupancy of the detection sites and Cl^- ions were refined, and the number of atoms were confirmed. In addition, the molar ratios of Zr^{4+} and Cl^- (2.7:1), which was quantitatively analyzed by ICP-OES and IC, respectively, matched the ratio of the chemical formula calculated from its X-ray crystal structure (3:1). In the crystal structure, the Cl^- was identified in the tetrahedral cage of the MOF on the symmetrically generated four sites with a partial occupancy (0.16) (Fig. 2e). Despite the limited space in the tetrahedral cage for the movement of Cl^-, the aperture and inner cavity size (3.50 and 6.3 Å) allowed the accommodation and exchange of Cl^- with the other ions, considering the size of the hydrated Cl^- ion (3.32 Å).

After the synthesis of the MOF-808-Cl, the excess Cl^- ions existed in the pores and was washed out using ion diffusion in water. The supernatant water containing the as-synthesized MOF-808-Cl powder had a high concentration of Cl^- (Fig. 2f). However, the amount of Cl^- released from the MOF-808-Cl powder remained similar even after repeated washing processes (Table S3). This result indicates that some Cl^- counter-ions bound to the MOF-808-Cl structure within the pore could be exchanged with water molecules, achieving ionic equilibrium with its surrounding media. This dynamic was also proved by the number of Cl^- ions released per mole of MOF increasing as the concentration of MOF-808-Cl in the water decreased (Fig. 2g). MOF-808-Cl particles should

release elevated amounts of Cl^- ions when their concentration is low to ensure ionic equilibrium in a certain amount of water. These results indicate that the sites previously occupied by Cl^- in the structure can be vacated in aqueous environments and that the Cl^- remaining in the structure can provide potential sites for ion exchange with other anions.

3.3. Ion removal performance in solutions containing Br^- or Cl^-

The ion removal performance of MOF-808-Cl was tested by immersing and penetrating the MOF powder and pellet in an aqueous solution containing either Br^- or Cl^-. For the penetration measurements, each powder and pellet sample were packed into cylindrical tubes, and an aqueous solution was introduced to flow throughout the samples. Specific concentrations of Br^- and Cl^- were prepared by diluting a 1,000-ppm standard solution for IC and measured by IC before and after MOF-808-Cl treatment.

We compared the ion removal performance of MOF-808-Cl for Br^- and Cl^-. The ion removal efficiency of immersion was evaluated in aqueous solutions containing only Br^- at initial concentrations of 1, 10, and 20 ppm or only Cl^- at 20 ppm. The MOF powder was immersed in 10 mL solution and removed after 2 h, and the remaining ion concentration was measured and compared with the initial concentration. When the amount of MOF-808-Cl was less than 50 mg, the Br^- the removal efficiency with the MOF amount increased sharply; however, above 50 mg, the slope of the increase flattened (Fig. 3a). The Br^- removal efficiency for the initial concentrations of 1 ppm was low (72.4 %), and was similar for higher initial concentrations (83.5 and 82.9 % for initial Br^- concentrations of 10 and 20 ppm, respectively, with 50 mg of MOF-808-Cl). However, the Cl^- removal efficiency with 50 mg of MOF-808-Cl was lower than the Br^- removal efficiency (82.9 %), reaching only 28.4 % for an initial concentration of 20 ppm. We speculated that the higher removal efficiency of Br^- occurred because it utilized both vacant site adsorptive and substitutional removal mechanisms. For the vacant site adsorption, the Zr-oxide units with a positive charge interacted initially with hydroxyl ions upon contact with water and subsequently exchanged with Br^- and Cl^- ions. However, only Br^- could also be removed substitutionally with existing Cl^- inside of MOF-808-Cl pores using its higher polarizability (Table 1) [23,24,26]. To determine the time required for sufficient Br^- removal, we tested its removal efficiency for varying immersion times in the 20 ppm Br^- solution. MOF-808-Cl powder (50 mg) was immersed for 1, 3, 5, 10, 30, 60, and 120 min, and the Br^- concentration was measured after removing the MOF. Within 1 min, the Br^- removal efficiency was 87.1 % and then remained constant, indicating that its removal rate is suitable for use in a flowing MOF filter system (Fig. 3b).

We analyzed the ion-exchange ratio between Cl^- and Br^- to understand the Br^- removal mechanism of MOF-808-Cl. This analysis was performed by comparing the initial and final concentrations across all

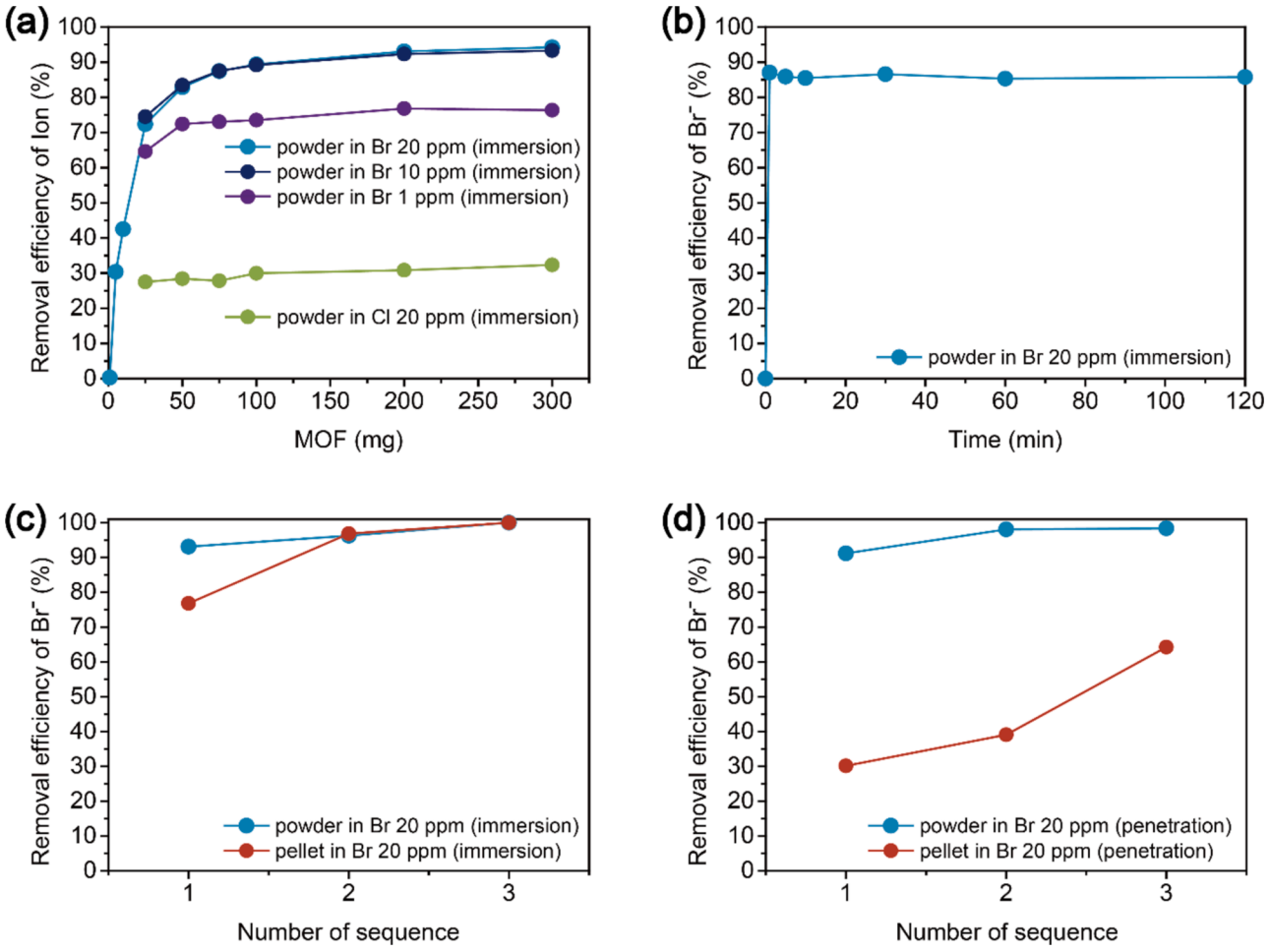

Fig. 3. Ion removal performance of MOF-808-Cl in solutions containing either Br^- or Cl^-. (a) Br^- removal efficiency of MOF powder (25, 50, 75, 100, 200, and 300 mg) in Br^--only solutions ($C_{i,Br}$: 1, 10, and 20 ppm; immersion system) and Cl^- removal efficiency of MOF powder in Cl^--only solutions ($C_{i,Cl}$: 20 ppm; immersion system). (b) Br^- removal efficiency of MOF powder in Br^--only solutions (contact time: 1, 3, 5, 10, 30, 60, and 120 min; $C_{i,Br}$: 20 ppm; immersion system). (c) Sequential tests for Br^- removal efficiency of MOF powder and pellet in Br^--only solutions ($C_{i,Br}$: 20 ppm; immersion system). (d) Sequential tests for Br^- removal efficiency of MOF powder and pellet in Br^--only solutions ($C_{i,Br}$: 20 ppm; penetration system).

measurement points, as shown in Fig. 3b. On average, the Br^- concentration decreased by 17.87 ppm, whereas the Cl^- concentration increased by 5.56 ppm (Table S4). Regarding the number of ions, every one Cl^- ion was released with the removal of 1.43 Br^- ions. Approximately 70 % of the Br^- was removed by the substitutional mechanism of defective sites, whereas the adsorption mechanism of vacant sites removed the remaining 30 %.

A sequential test was also conducted to demonstrate complete removal in repeated immersion processes with both powder and pellet samples. Each MOF-808-Cl powder (1 g) and pellet (1 g) sample was tested in separate batches by immersing them in Br^- 20 ppm solutions for 2 h. The Br^- removal efficiency was then determined by comparing the initial and final concentrations after each sequence. After three steps, the Br^- removal efficiency was 100 % for both powder and pellet samples (Fig. 3c). The Br^- removal efficiency for each step decreased with the sequential process (Table S5), which aligned with the results observed for the lower initial concentrations in Fig. 3a. Furthermore, the particle density of the pellet was controlled by applying pressure in pelletizing process to investigate the effect of packing density on the Br^- removal efficiency. The results in Table S6 showed that the higher packing density of the pellet has the lower efficiency. The pellets having the packing density higher than 1 g/cm^3 showed the similar removal efficiency. A penetrating sequential test was performed to evaluate the Br^- removal performance under practical conditions where fluids flowed through the materials. Each powder (50 mg) and pellet (1.0 g) sample of MOF-808-Cl was packed into a syringe and passed through a 20 ppm Br^- solution. The existing solution was then introduced into another syringe filled with the MOF samples that had not been exposed to the solution. After each sequence, the Br^- concentration in the filtered solution was compared with the initial concentration. For the powder samples, the Br^- removal efficiencies were 91.2, 98.1, and 98.4 % in the first, second, and third steps, respectively. However, the pellets exhibited lower efficiencies of 30.1, 39.1, and 64.3 % (Fig. 3d). The low efficiency for the pellets likely resulted from the void inter-pellet space, which did not provide sufficient contact opportunities for Br^- ions. Even though a smaller amount of powder (50 mg) was used compared with larger amounts of pellets (1.0 g), the flow resistance during penetration was much lower for the pellets, resulting in a faster solution passage. Consequently, the opportunities for adequate contact between Br^- and the pellet surface were insufficient, thereby limiting the removal efficiency. This issue must be addressed when optimizing the pellet size and packing density in future processes. Additionally, the sequential tests focused on determining the number of processes needed for complete Br^- removal. To enhance reusability of the MOF-808-Cl, future studies should explore regeneration methods, such as mild chemical treatments or controlled thermal processes, to preserve the MOF-808-Cl's structural and functional integrity for practical applications.

3.4. Selective Br^- removal performance in Cl^--dominated solution

To investigate whether Br^- could be effectively removed from Cl^--dominated solutions, the solutions containing Cl^- (100 ppm) and Br^- (20 ppm or lower) were prepared. This was achieved by preparing individual solutions of Cl^- (200 ppm) and Br^- (40 ppm or lower) and

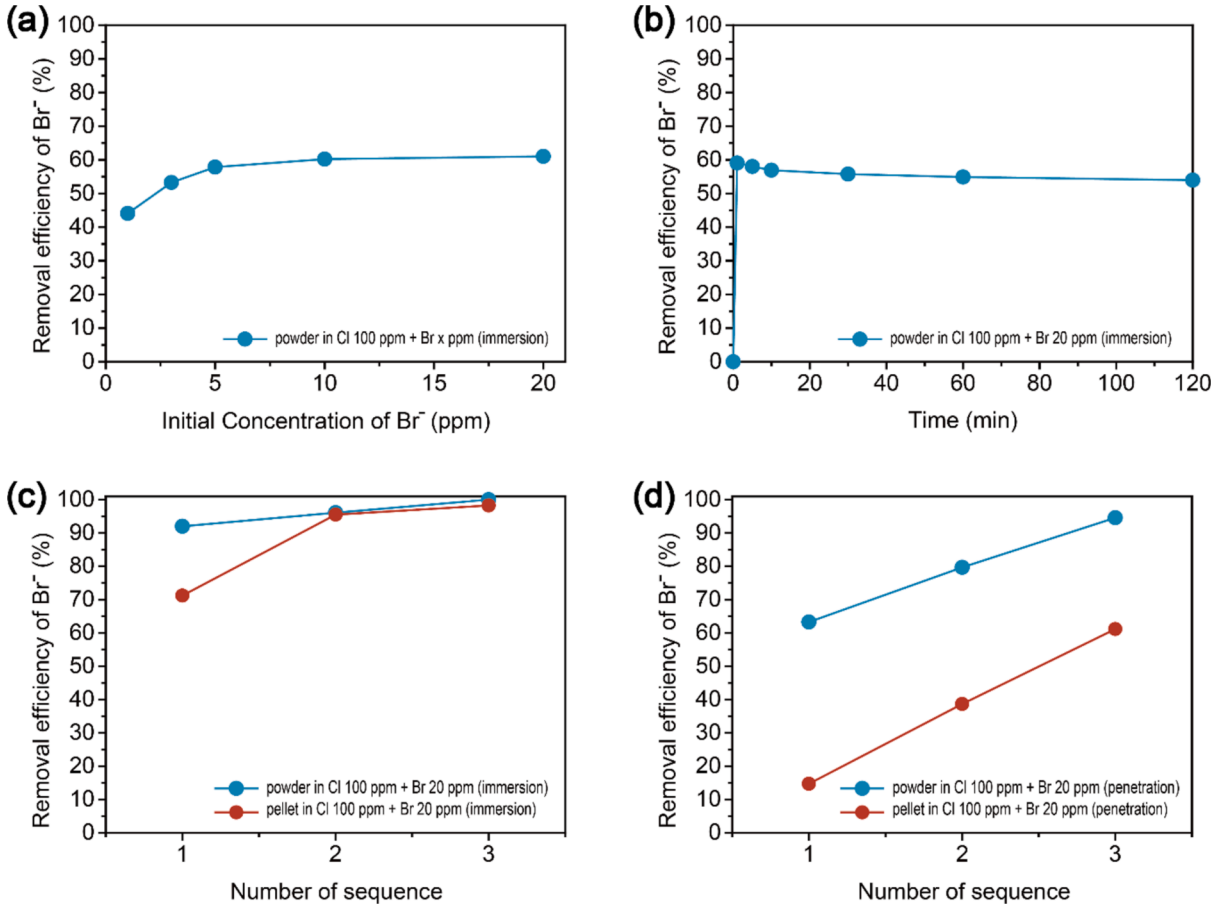

Fig. 4. Br^- removal performance of MOF-808-Cl in Cl^--dominated solutions. (a) Br^- removal efficiency of MOF powder at various initial Br^- concentrations ($C_{i,Br}$: 1, 3, 5, 10, and 20 ppm; $C_{i,Cl}$: 100 ppm; immersion system). (b) Br^- removal efficiency of MOF powder in various process time (contact time: 1, 3, 5, 10, 30, 60, and 120 min; $C_{i,Br}$: 20 ppm; $C_{i,Cl}$: 100 ppm; immersion system). (c) Sequential tests for Br^- removal efficiency of MOF powder and pellets ($C_{i,Br}$: 20 ppm; $C_{i,Cl}$: 100 ppm; immersion system). (d) Sequential tests for Br^- removal efficiency of MOF powder and pellets ($C_{i,Br}$: 20 ppm; $C_{i,Cl}$: 100 ppm; penetration system).

mixing them. The Br^- removal performance was also tested by immersing and penetrating MOF-808-Cl powder and pellet samples in the mixed solution, following the same procedure outlined in Section 3.3.

The Cl^- (200 ppm) and Br^- (2, 6, 10, 20, and 40 ppm) solutions were mixed to make 1, 3, 5, 10, and 20 ppm of Br^- in the solution containing 100 ppm of Cl^-. The Br^- removal efficiencies of the 50 mg of powder sample were 44.1, 53.2, 57.8, 60.2, and 61.0 % for the initial concentrations of 1, 3, 5, 10, and 20 ppm Br^- in the presence of 100 ppm Cl^-, respectively (Fig. 4a). These results indicate that Br^- was successfully removed selectively even in the presence of Cl^--dominated solutions. The removal efficiency of Br^- was lower (61.0 % at 20 ppm Br^-) compared to that when only Br^- was present (Fig. 3a); this difference likely occurred because Br^- can only be removed by the substitution mechanism in the dominated presence of Cl^-. Some Cl^- was also removed from the solution probably using the ion-adsorption mechanism. To determine the time required for Br^- removal in a Cl^--dominated solution, we assessed Br^- removal efficiency over different immersion times in a solution containing both Cl^- (100 ppm) and Br^- (20 ppm). MOF-808-Cl powder (50 mg) was immersed for 1, 3, 5, 10, 30, 60, and 120 min, and Br^- concentration was measured after MOF was removed. The Br^- removal efficiency was 59.1 % within 1 min and then remained similar (Fig. 4b). This result suggests that the required time for Br^- removal remained similar with the Br^- only condition (Fig. 3b), even under Cl^--dominated conditions. In addition, we performed a sequential test with the powder and pellet forms of MOF-808-Cl. In the immersion-type measurements, the removal efficiencies reached 100 % for the powder and 98.3 % for the pellets after three sequences (Fig. 4c). In the penetration measurement, the Br^- removal efficiencies were 94.6 and 61.1 % for powder and pellet samples, respectively, after the third step (Fig. 4d). Despite the dominant presence of Cl^-, the Br^- removal using the MOF-808-Cl were successful, and their kinetic and sequential performances were comparable to those observed when only Br^- was present.

4. Conclusions

This study demonstrated the selective removal of bromide ions (Br^-) from chloride ions (Cl^-)-dominated solutions using the defect sites of MOF-808-Cl. Structural analysis confirmed the presence of Cl^- in defect sites of MOF-808-Cl, and subsequent experiments with both powder and pellet forms indicated a preferential removal of Br^- over Cl^- in aqueous environments. The removal mechanism was identified as a combination of vacant-site adsorption (30 %) and substitutional removal (70 %) leveraging the differences in polarizability between the two ions. Notably, effective Br^- removal occurred even in conditions where the concentration of Cl^- was 100 times greater than that of Br^-. These findings highlight the potential of MOF-808-Cl as an effective material for the selective extraction of Br^- from complex ionic solutions, thereby facilitating further advancements in water treatment technologies.

CRediT authorship contribution statement

WooYeon Moon: Writing – original draft, Visualization, Validation, Methodology, Investigation, Formal analysis, Conceptualization. **Dong Gyu Park:** Methodology, Conceptualization. **Younghu Son:** Software, Formal analysis. **Minyoung Yoon:** Writing – original draft, Software, Investigation, Formal analysis. **Kyung Min Choi:** Writing – review & editing, Supervision, Project administration.

Declaration of competing interest

The authors declare that they have no known competing financial interests or personal relationships that could have appeared to influence the work reported in this paper.

Acknowledgements

This study was supported by the National Research Foundation of Korea (NRF) grants funded by the Korean Government (MSIT) (Nos. 2022R1A2B5B01001826, 2022R1A5A2021216, RS-2023-00218255 and RS-2023-00254645). The single-crystal diffraction X-ray experiments at the PAL 2D-SMC beamline were supported by the Ministry of Science and ICT.

Appendix A. Supplementary material

Supplementary data to this article can be found online at https://doi.org/10.1016/j.apsusc.2025.162309.

Data availability

No data was used for the research described in the article.

References

[1] A.C. Leri, O. Hettithanthri, S. Bolan, T. Zhang, J. Unrine, S. Myneni, D.R. Nachman, H.T. Tran, A.J. Phillips, D. Hou, Y. Wang, M. Vithanage, L.P. Padhye, T. Jasemi Zad, A. Heitz, K.H.M. Siddique, H. Wang, J. Rinklebe, M.B. Kirkham, N. Bolan, Bromine contamination and risk management in terrestrial and aquatic ecosystems, J. Hazard. Mater. 469 (2024) 133881, https://doi.org/10.1016/j.jhazmat.2024.133881.

[2] C.M. Morrison, S. Hogard, R. Pearce, A. Mohan, A.N. Pisarenko, E.R.V. Dickenson, U. von Gunten, E.C. Wert, Critical review on bromate formation during ozonation and control options for its minimization, Environ. Sci. Tech. 57 (2023) 18393–18409, https://doi.org/10.1021/acs.est.3c00538.

[3] X. Wu, L. Li, B. Li, Z. Wang, Y. Wu, Current status and future trends of high-temperature gas environment corrosion on metal coatings in solid waste incinerators, Process Saf. Environ. Prot. 191 (2024) 146–162, https://doi.org/10.1016/j.psep.2024.08.116.

[4] A. Mills, H. Davies, Kinetics of corrosion of ruthenium dioxide hydrate by bromate ions under acidic conditions, J. Chem. Soc. Faraday Trans. 86 (1990) 955–958, https://doi.org/10.1039/FT9908600955.

[5] Y. Chen, C.-J. Yuan, B.-J. Xu, J.-Y. Cao, M.-Y. Lee, M. Liu, Q. Wu, Y. Du, Suppressing organic bromine but promoting bromate: is the ultraviolet/ozone process a double-edged sword for the toxicity of wastewater to mammalian cells? Environ. Sci. Tech. 58 (2024) 11649–11660, https://doi.org/10.1021/acs.est.4c00329.

[6] K. Watson, M.J. Farré, N. Knight, Strategies for the removal of halides from drinking water sources, and their applicability in disinfection by-product minimisation: a critical review, J. Environ. Manag. 110 (2012) 276–298, https://doi.org/10.1016/j.jenvman.2012.05.023.

[7] F. Valero, R. Arbós, Desalination of brackish river water using Electrodialysis Reversal (EDR), Desalination 253 (2010) 170–174, https://doi.org/10.1016/j.desal.2009.11.011.

[8] J. Egitto, J. Latayan, S. Pagsuyoin, O. Apul, E. Agar, Towards selective removal of bromide from drinking water resources using electrochemical desalination, Chem. Eng. J. Adv. 12 (2022) 100369, https://doi.org/10.1016/j.ceja.2022.100369.

[9] P. Xu, J.E. Drewes, D. Heil, G. Wang, Treatment of brackish produced water using carbon aerogel-based capacitive deionization technology, Water Res. 42 (2008) 2605–2617, https://doi.org/10.1016/j.watres.2008.01.011.

[10] I. Cohen, B. Shapira, E. Avraham, A. Soffer, D. Aurbach, Bromide ions specific removal and recovery by electrochemical desalination, Environ. Sci. Tech. 52 (2018) 6275–6281, https://doi.org/10.1021/acs.est.8b00282.

[11] C. Gong, Z. Zhang, Q. Qian, D. Liu, Y. Cheng, G. Yuan, Removal of bromide from water by adsorption on silver-loaded porous carbon spheres to prevent bromate formation, Chem. Eng. J. 218 (2013) 333–340, https://doi.org/10.1016/j.cej.2012.12.059.

[12] C. Chen, O.G. Apul, T. Karanfil, Removal of bromide from surface waters using silver impregnated activated carbon, Water Res. 113 (2017) 223–230, https://doi.org/10.1016/j.watres.2017.01.019.

[13] A.E. Al-Rawajfeh, A.I. Alrawashdeh, M.T. Etiwi, A. Alnawaiseh, M.K. Shahid, M.H. M. Masad, S.O. Oran, S.F. Alshahateet, Silver nanoparticles (Ag-NPs) embedded in zeolite framework: a comprehensive study on bromide removal from water, including characterization, antibacterial properties, and adsorption mechanisms, Desalin. Water Treat. 317 (2024) 100139, https://doi.org/10.1016/j.dwt.2024.100139.

[14] M. Soyluoglu, M.S. Ersan, M. Ateia, T. Karanfil, Removal of bromide from natural waters: bromide-selective vs. conventional ion exchange resins, Chemosphere 238 (2020) 124583, https://doi.org/10.1016/j.chemosphere.2019.124583.

[15] S. Hsu, P.C. Singer, Removal of bromide and natural organic matter by anion exchange, Water Res. 44 (2010) 2133–2140, https://doi.org/10.1016/j.watres.2009.12.027.

[16] F. Ge, L. Zhu, Effects of coexisting anions on removal of bromide in drinking water by coagulation, J. Hazard. Mater. 151 (2008) 676–681, https://doi.org/10.1016/j.jhazmat.2007.06.041.

[17] G.V. Zoccolante, High-Purity Water, in: Good Design Practices for GMP Pharmaceutical Facilities, second ed., CRC Press, 2016. https://doi.org/10.1201/9781315372242.
[18] M. Sun, G.V. Lowry, K.B. Gregory, Selective oxidation of bromide in wastewater brines from hydraulic fracturing, Water Res. 47 (2013) 3723–3731, https://doi.org/10.1016/j.watres.2013.04.041.
[19] X. Wang, D. Xu, D. Yu, J. Liang, X. Liang, Q. Shou, Fe-doped Zr-based metal-organic frameworks for efficient bromide ion capture: adsorption performance and mechanism, J. Environ. Chem. Eng. 12 (2024) 111600, https://doi.org/10.1016/j.jece.2023.111600.
[20] R. Mahesh, K. Vora, M. Hanumanthaiah, A. Shroff, P. Kulkarni, S. Makuteswaran, S. Ramdas, H.L. Ramachandraih, A.V. Raghu, Removal of pollutants from wastewater using alumina based nanomaterials: a review, Korean J. Chem. Eng. 40 (2023) 2035–2045, https://doi.org/10.1007/s11814-023-1419-x.
[21] R. Boopathy, A. Gnanamani, A.B. Mandal, G. Sekaran, A first report on the selective precipitation of sodium chloride from the evaporated residue of reverse osmosis reject salt generated from the leather industry, Ind. Eng. Chem. Res. 51 (2012) 5527–5534, https://doi.org/10.1021/ie201735s.
[22] B. Min, H. Chung, T. Kim, J. Park, Study on disinfection by-products formation according to kind of salt in on-site production, J. Korean Soc. Water Wastewater 29 (2015) 575–581, https://doi.org/10.11001/jksww.2015.29.5.575.
[23] H. Wang, X. Han, Y. Chen, W. Guo, W. Zheng, N. Cai, Q. Guo, X. Zhao, F. Wu, Effects of F^-, Cl^-, Br^-, NO_3^-, and SO_4^{2-} on the colloidal stability of Fe_3O_4 nanoparticles in the aqueous phase, Sci. Total Environ. 757 (2021) 143962, https://doi.org/10.1016/j.scitotenv.2020.143962.
[24] S. Yoo, Y.A. Lei, X.C. Zeng, Effect of polarizability of halide anions on the ionic solvation in water clusters, J. Chem. Phys. 119 (2003) 6083–6091, https://doi.org/10.1063/1.1601609.
[25] P.-H. Chang, C.-Y. Chen, R. Mukhopadhyay, W. Chen, Y.-M. Tzou, B. Sarkar, Novel MOF-808 metal–organic framework as highly efficient adsorbent of perfluorooctane sulfonate in water, J. Colloid Interface Sci. 623 (2022) 627–636, https://doi.org/10.1016/j.jcis.2022.05.050.
[26] G.M. Geise, H.J. Cassady, D.R. Paul, B.E. Logan, M.A. Hickner, Specific ion effects on membrane potential and the permselectivity of ion exchange membranes, Phys. Chem. Chem. Phys. 16 (2014) 21673–21681, https://doi.org/10.1039/C4CP03076A.
[27] S. Jang, S. Jee, R. Kim, J.H. Lee, H.Y. Yoo, W. Park, J. Shin, K.M. Choi, Heterojunction of pores in granola-type crystals of two different metal–organic frameworks for enhanced formaldehyde removal, Bull. Kor. Chem. Soc. 42 (2021) 315–321, https://doi.org/10.1002/bkcs.12185.
[28] J. Kim, C. Na, Y. Son, M. Prabu, M. Yoon, Stilbene ligand-based metal–organic frameworks for efficient dye adsorption and nitrobenzene detection, Bull. Kor. Chem. Soc. 44 (2023) 507–515, https://doi.org/10.1002/bkcs.12683.
[29] J.F. Kurisingal, J.H. Choe, H. Kim, J. Youn, G. Cheon, C.S. Hong, Post-synthetic modifications of MOF-74 type frameworks for enhancing CO capture and moisture stability, Bull. Kor. Chem. Soc. 45 (2024) 675–688, https://doi.org/10.1002/bkcs.12885.
[30] G. Lee, S. Oh, M. Oh, Enhanced early-stage adsorption of chemical warfare agent simulant by MIL-68-(X%OH), Bull. Kor. Chem. Soc. 45 (2024) 67–73, https://doi.org/10.1002/bkcs.12794.
[31] J. Zhang, J. Ma, C. Liu, Q. Wang, Y. Xu, L. Fang, K. Xia, D. Sun, Bio-base metal organic frameworks as potential CO_2 adsorbents, Korean J. Chem. Eng. 41 (2024) 2099–2107, https://doi.org/10.1007/s11814-024-00201-6.
[32] T.N. Tu, N.T. Tran, Q.H. Nguyen, V.N. Le, J. Kim, Metal–organic frameworks for aromatic-based VOC decomposition, Korean J. Chem. Eng. 41 (2024) 2461–2476, https://doi.org/10.1007/s11814-024-00199-x.
[33] M. Amidi, E. Salehi, ZIF-8 derived porous carbon/ZnO as an effective nanocomposite adsorbent for removal of acetic acid, Korean J. Chem. Eng. 40 (2023) 2384–2395, https://doi.org/10.1007/s11814-023-1492-1.
[34] K.D. Nguyen, P.H. Ho, P.D. Vu, T.L.D. Pham, P. Trens, F. Di Renzo, N.T.S. Phan, H. V. Le, Efficient removal of Chromium(VI) anionic species and dye anions from water using MOF-808 materials synthesized with the assistance of formic acid, Nanomaterials 11 (2021) 1398, https://doi.org/10.3390/nano11061398.
[35] X. Li, L. Huang, A. Kochubei, J. Huang, W. Shen, H. Xu, Q. Li, Evolution of a metal-organic framework into a Brønsted acid catalyst for glycerol dehydration to acrolein, ChemSusChem 13 (2020) 5073–5079, https://doi.org/10.1002/cssc.202001377.
[36] T. Wang, H. Zhao, X. Zhao, Q. Yang, D. Liu, Silver nanoparticles prepared by one-step reaction via reducibility of a metal–organic framework to remove the toxic bromine ions, J. Chem. Eng. Data 66 (2021) 535–543, https://doi.org/10.1021/acs.jced.0c00774.
[37] A.H. Valekar, S.-K. Lee, Y.K. Kim, K.H. Cho, D. Jo, Y.K. Hwang, J.W. Yoon, U.-H. Lee, Facile shaping of flexible MIL-53(Al) for effective separation of propylene over propane, Chem. Eng. J. 480 (2024) 147872, https://doi.org/10.1016/j.cej.2023.147872.
[38] J. Zheng, X. Cui, Q. Yang, Q. Ren, Y. Yang, H. Xing, Shaping of ultrahigh-loading MOF pellet with a strongly anti-tearing binder for gas separation and storage, Chem. Eng. J. 354 (2018) 1075–1082, https://doi.org/10.1016/j.cej.2018.08.119.
[39] U. Ryu, S. Jee, P.C. Rao, J. Shin, C. Ko, M. Yoon, K.S. Park, K.M. Choi, Recent advances in process engineering and upcoming applications of metal–organic frameworks, Coord. Chem. Rev. 426 (2021) 213544, https://doi.org/10.1016/j.ccr.2020.213544.
[40] H. Furukawa, F. Gándara, Y.-B. Zhang, J. Jiang, W.L. Queen, M.R. Hudson, O. M. Yaghi, Water adsorption in porous metal–organic frameworks and related materials, J. Am. Chem. Soc. 136 (2014) 4369–4381, https://doi.org/10.1021/ja500330a.
[41] J.W. Shin, K. Eom, D. Moon, BL2D-SMC, the supramolecular crystallography beamline at the Pohang Light Source II, Korea, J. Synchrotron Rad. 23 (2016) 369–373, https://doi.org/10.1107/S1600577515021633.
[42] Z. Otwinowski, D. Borek, W. Majewski, W. Minor, Multiparametric scaling of diffraction intensities, Acta Cryst. A 59 (2003) 228–234, https://doi.org/10.1107/S0108767303005488.
[43] J. Lübben, C.M. Wandtke, C.B. Hübschle, M. Ruf, G.M. Sheldrick, B. Dittrich, Aspherical scattering factors for SHELXL – model, implementation and application, Acta Cryst. A 75 (2019) 50–62, https://doi.org/10.1107/S2053273318013840.
[44] H. He, L. Hashemi, M.-L. Hu, A. Morsali, The role of the counter-ion in metal-organic frameworks' chemistry and applications, Coord. Chem. Rev. 376 (2018) 319–347, https://doi.org/10.1016/j.ccr.2018.08.014.
[45] C. Ardila-Suárez, H. Alem, V.G. Baldovino-Medrano, G.E. Ramírez-Caballero, Synthesis of ordered microporous/macroporous MOF-808 through modulator-induced defect-formation, and surfactant self-assembly strategies, Phys. Chem. Chem. Phys. 22 (2020) 12591–12604, https://doi.org/10.1039/D0CP00287A.
[46] Z. Lu, J. Duan, L. Du, Q. Liu, N.M. Schweitzer, J.T. Hupp, Incorporation of free halide ions stabilizes metal–organic frameworks (MOFs) against pore collapse and renders large-pore Zr-MOFs functional for water harvesting, J. Mater. Chem. A 10 (2022) 6442–6447, https://doi.org/10.1039/D1TA10217F.